Master Equation Models for the Pressure- and Temperature-Dependent Reactions HO + NO_2 → $HONO_2$ and HO + NO_2 → HOONO

David M. Golden,*,† John R. Barker,*,‡,§ and Lawrence L. Lohr*,§

Department of Mechanical Engineering, Stanford University, Stanford, California 94305, Department of Atmospheric, Oceanic and Space Sciences, University of Michigan, Ann Arbor, Michigan 48109-2143, and Department of Chemistry, University of Michigan, Ann Arbor, Michigan 48109-1055

Received: May 13, 2003; In Final Form: September 22, 2003

Data for the reactions between OH and NO_2 have been modeled using a multiwell, multichannel master equation approach. In this work, new ab initio quantum chemical results for *cis*−*cis*- and *trans*−*perp*-HOONO at the QCISD(T)/cc-pVDZ level are used with the multiple-well, multiple-channel master equation approach in order to model the data between 220 and 430 K in both He and N_2. The results are in good agreement with the experimental data over the entire ranges of temperature and pressure. The contribution from HOONO is evaluated for the experimental conditions. It is also evaluated for the conditions described by the U.S. Standard Atmosphere (1976). Although the $HONO_2$ pathway dominates over all atmospheric conditions, up to ∼20% of the reaction is predicted to yield HOONO near the tropopause. If the atmospheric fate of HOONO is different than that of $HONO_2$, this can affect atmospheric chemistry models.

Introduction

The reaction of OH with NO_2 is the principal sink for NO_x in the troposphere and thus has a direct effect on ozone production. In the stratosphere, nitric acid ($HONO_2$) is a "reservoir species", which "stores" highly reactive OH and NO_2 in a relatively inert form. In addition, the reaction is a popular test bed for investigating fundamental aspects of recombination reactions. In experiments, OH radical can be detected with high sensitivity on very short time scales under an exceptionally wide range of experimental conditions. This has enabled experiments at temperatures from ∼220 to ∼450 K and pressures from ∼1 mbar to ∼1 kbar. The experimental data have been reviewed elsewhere.[1,2] Recent experiments have shown unambiguous evidence for the existence[3] and significant production of peroxynitrous acid (HOONO),[4] although its existence had been surmised earlier.[5−7] Recent spectroscopic results[8−10] have confirmed the existence of HOONO. Thus the reaction can be written with two channels

$$\mathrm{OH} + \mathrm{NO_2} \rightarrow \mathrm{HONO_2} \quad (1a)$$

$$\rightarrow \mathrm{HOONO} \quad (1b)$$

These reactions are precisely analogous to the reactions forming alkyl nitrates from alkoxy radicals reacting with NO_2. Furthermore, ROONO (where R is an alkyl group) has been implicated in the formation of alkyl nitrates from the reactions of RO_2 radicals with nitric oxide.[11−13] Several theoretical models of this system have been reported recently.[14−16]

Even when experimental data are unusually extensive, theoretical models must be used to assist in estimating the rate data needed for modeling the atmosphere, combustion, and other complex chemical systems. Thus much work has been aimed at modeling "elementary" chemical reactions. Part of the motivation of such work has been a desire to test the limits of knowledge of elementary reactions. For the most reliable interpolation and extrapolation, it is necessary to employ the best theoretical methods that can be applied to the system. In the past few years, this reaction system has been analyzed theoretically by several groups.

Chakraborty et al.[17] carried out ab initio electronic structure calculations and applied the results by using canonical variational Rice−Ramsperger−Kassel−Marcus (RRKM) theory to obtain rate constants in reasonable agreement with the experimental data. Golden and Smith[7] used RRKM theory to reexamine the reaction system in light of recent experimental and theoretical information. Matheu and Green[18] investigated the reaction system by using literature ab initio results and an inverse Laplace transform representation of the energy-dependent rate constants. Troe[19] also carried out a reanalysis of the reaction in light of recent new data on the reaction system.

The present work differs from the previous theoretical work in several ways. First, a multichannel, multiwell master equation analysis was carried out. Second, additional high-level ab initio electronic structure calculations were carried out and utilized with the master equation. Third, a unified model was found that satisfactorily describes all of the existing experimental kinetics data. The unified model is used to generate practical formulas for calculating rate constants as functions of temperature and pressure for use in atmospheric chemistry models. Finally, the model is used to estimate the fractional yield of HOONO as a function of altitude in the earth's atmosphere.

Experimental Data

There is a large body of experimental data for this system.[4,20−26] Much of it has been discussed in recent publications.[7,18,19] The data from Hippler and co-workers cleverly separates the two pathways forming $HONO_2$ and HOONO at 430 K and very high pressures (up to 130 bar).[4]

* Address correspondence to any author: david.golden@stanford.edu (D.M.G.); jrbarker@umich.edu (J.R.B.); llohr@umich.edu (L.L.L.).

† Stanford University.

‡ Department of Atmospheric, Oceanic and Space Sciences, University of Michigan.

§ Department of Chemistry, University of Michigan.

10.1021/jp0353183 CCC: $25.00
Published on Web 11/14/2003

TABLE 1: Energies[a] of HOONO Conformers Relative to Planar *cis-cis* HOONO

level	cis−perp	TS1[b]	TS2[c]	trans−perp
B3LYP/6-311++G**	0.8	1.9	56.3, 59.8	8.1
G2	5.6			13.3
G3	5.6	5.5	59.5, 62.1	13.5
QCISD(T)/cc-pVDZ[d]	5.0	4.4	61.0, 63.3	15.7
QCISD(T)/6-311G(d,p)[e]	2.9			11.7

[a] $\Delta U°$ (0 K) in kJ mol^{-1} including zero-point energies. [b] Transition state connecting cis−perp and cis−cis via rotation about the O−O bond. [c] Pair of transition states connecting trans−perp and cis−cis via rotation about the N−O bond. [d] Values using QCISD(T)/cc-pVDZ zero-point energies. [e] McGrath and Rowland (ref 27) with MP2/6-31G(d) geometries and frequencies.

Quantum Chemical Results

Characterization of HOONO and $HONO_2$. Our kinetics modeling requires information about the overall thermochemistry of HOONO/$HONO_2$ formation from OH and NO_2, the isomerization between HOONO conformers, and the isomerization of HOONO to $HONO_2$, as well as geometries and vibrational frequencies of equilibrium structures. A large number of quantum chemical studies of the HOONO/$HONO_2$ system have been reported.[27−40] Especially thorough studies have been those of McGrath and Rowland,[28] Houk et al.,[37] Sumathi and Peyerimhoff,[38] Li and Francisco,[39] and Dixon et al.[40] McGrath and Rowland[28] obtained at the QCISD(T)6-311G(d,p)//MP2/6-31G(d) level values of 2.9 and 11.7 kJ mol^{-1}, respectively, for $\Delta U°$ (0 K), including zero-point energy (ZPE) contributions, of the cis−perp and trans−perp conformers of HOONO relative to that of the planar cis−cis conformer. As noted in several earlier investigations, the planar cis−cis conformer of HOONO with C_s symmetry is favored over nonplanar conformers at essentially all levels of computation that include electron correlation. The nonplanar cis−perp conformer, in which the OONO portion of the molecule is cis and nearly planar while the bond to H is nearly normal to this plane, is of marginal stability as a local minimum. By contrast, the nonplanar trans−perp conformer, in which the OONO portion of the molecule is trans and nearly planar while the bond to H is nearly normal to this plane, appears on the basis of many calculations to be a well-defined local minimum. Our best values for $\Delta U°$ (0 K) for these conformers (Table 1, obtained using the Gaussian 94 and Gaussian 98 programs),[41,42] namely, 5.0 and 15.7 kJ mol^{-1}, respectively, at the QCISD(T)/cc-pVDZ level, are slightly higher than those of McGrath and Rowland. Nonetheless our results support the conclusion of Dixon et al.[40] that the nonplanar cis−perp structure may well not be a local minimum. Our results (Table 1) show that the intrinsic energy barrier connecting cis−perp and cis−cis via rotation about the O−O bond is negligible. The energy of this saddle point (including ZPEs) is actually slightly below that of the cis−perp minimum (including ZPEs), although its electronic energy is slightly higher, namely, by 1.8, 0.5, and 0.2 kJ mol^{-1} at the B3LYP/6-311++G**, G3, and QCISD(T)/cc-pVDZ levels, respectively. Even if the cis−perp structure is bound, the binding energy is so small that the structure will not have significant population at the temperatures of interest here. Thus we shall treat HOONO as having only the planar cis−cis and nonplanar trans−perp minima, which are connected by pathways involving rotation about both the N−O and O−O bonds. We have located a pair of closely related transition states on these pathways with energies (Table 1) of 61.0 and 63.3 kJ mol^{-1}, respectively, at the QCISD(T)/cc-pVDZ level. As the structures and vibrational frequencies of the pair are quite similar (Tables2 and 3), essentially differing only in the sign of the N−O−O−H dihedral angle, we have simplified our kinetic modeling by considering only one set of transition state parameters and assuming the path is doubly degenerate (taking into account the two directions of twist about the N−O bond in going from trans−perp to cis−cis).

TABLE 2: Structures[a] of HOONO Conformers

parameter	cis−cis	TS_2[b]	trans−perp
R(O−N)	1.197	1.159, 1.162	1.175
R(N−O)	1.412	1.656, 1.645	1.504
R(O−O)	1.443	1.448, 1.448	1.442
R(O−H)	0.980	0.974, 0.974	0.974
A(O−N−O)	113.9	109.4, 109.4	108.6
A(N−O−O)	112.8	99.2, 99.3	104.9
A(O−O−H)	99.6	100.1, 100.0	100.1
D(O−N−O−O)	0.0	82.9, 91.4	176.5
D(N−O−O−H)	0.0	97.9, −95.6	98.6

[a] Bond distances in angstroms and angles in degrees at the QCISD(T)/cc-pVDZ level. [b] Pair of transition states connecting trans−perp and cis−cis via rotation about the N−O bond. [c] The planar $HONO_2$ structure at the QCISD(T)/cc-pVDZ level has R(N−O1) = 1.417, R(N−O2) = 1.218, R(N−O3) = 1.204, R(H−O1) = 0.977, A(O1−N−O2) = 115.5, A(O1−N−O3) = 115.5, and A(H−O1−N) = 101.3.

TABLE 3: Vibrational Frequencies (cm^{-1})[a,b] of HOONO Conformers and $HONO_2$

mode	cis−cis	trans−perp	TS2[c]	$HONO_2$
ν1	363*	206	224 i, 218 i	477*
ν2	397	293	272, 278	576
ν3	515*	353	374, 381	644
ν4	618	442	434, 416	762*
ν5	796	774	661, 687	892
ν6	939	951	853, 854	1337
ν7	1461	1392	1353, 1355	1360
ν8	1649	1758	1816, 1797	1786
ν9	3496	3753	3744, 3732	3738

[a] Vibrational wavenumbers in cm^{-1} in at the QCISD(T)/cc-pVDZ level. [b] Values marked with an asterisk are for "a" modes of planar structures. [c] Pair of transition states connecting trans−perp and cis−cis via rotation about the N−O bond. The first entry of each row was used for RRKM calculations of the isomerization rate constant. In addition, mode ν_2 was treated as a 2-fold internal rotor with reduced moment of inertia equal to 0.919 amu Å^2. The resulting A factor for isomerization (in the trans → cis direction) is 1.8×10^{13} s^{-1}.

The studies of Houk et al.[37] and Sumathi and Peyerimhoff[38] are largely based on DFT methods, which yield very reasonable values for conformational energies but not very good values for bond-breaking energies. Li and Francisco[39] carried out a very thorough study of the structure and stability of HOONO, obtaining at the QCISD(T)/cc-pVQZ level dissociation energies of 78.6 and 105.0 kJ mol^{-1} to form OH + NO_2 and HO_2 + NO, respectively. Dixon et al.[40] followed this by examining various decomposition pathways for HOONO. They also reported a transition state for the isomerization of HOONO to $HONO_2$ having an energy at the CCSD(T)/CBS//MP2/cc-pVDZ level (CBS denotes extrapolation of aug-cc-pVXZ results, X = D, T, Q, to the complete basis set limit) of 89.5 kJ mol^{-1} above that for HOONO and with a structure corresponding to a weakly bound adduct of OH and NO_2. (The distance from N to the O of OH is 2.784 Å.) At this same level the energy of OH + NO_2 is 82.8 kJ mol^{-1} above that of HOONO so the isomerization transition state energy is about 6.7 kJ mol^{-1} above that of OH + NO_2.

Related studies of the corresponding alkyl systems include those of Zhang et al.,[14] Lohr et al.,[15] and Ellison et al.[43] The transition state reported by Ellison et al. for the methyl system is quite different from that reported by Dixon et al.[40] for the hydrogen system. On the basis of their coupled-cluster electronic

TABLE 4: Energies[a] of HOONO and OH + NO_2 Relative to $HONO_2$

level	HOONO	OH + NO_2
B3LYP/6-311++G**	129.2	174.6
G2	119.9	204.7
G3	121.7	194.6
QCISD(T)/cc-pVDZ	104.0	165.5
QCISD(T)/cc-pVTZ[b]	111.2	188.4
CCSD(T)/CBS[c]	121.2	204.1
Exp.	114.1 ± 1[d]	197.3

[a] $\Delta U°$ (0 K) in kJ mol^{-1} including zero-point energies. [b] Values using the QCISD(T)/cc-pVDZ zero-point energies. [c] Dixon et al. (ref 39). [d] Hippler et al. (ref 4).

structure calculations Ellison et al. report a barrier of 80−120 kJ mol^{-1} for the isomerization of CH_3OONO to CH_3ONO_2, an energy not much below that for fragmentation to CH_3OO and NO. Zhang et al.[14] and Lohr et al.[15] did not compute a transition state but analyzed the available experimental data considering a range of transition state parameters.

Isomerization of $HONO_2$ to HOONO and Dissociation to OH and NO_2. We present in Table 4 computed values of the energy difference between HOONO and $HONO_2$, with all values including zero-point energy contributions. Compared to the recent experimental estimate of 114 ± 1 kJ mol^{-1} by Hippler et al.[4] and the revised value of 116 ± 1 kJ mol^{-1} shown in the present work (Appendix), the B3LYP/6-311++G** value is about 15 kJ mol^{-1} too high, while the G2 and G3 values are only about 5 kJ mol^{-1} too high, as is the CCSD(T)/CBS value of Dixon et al.[40] Somewhat too small is our QCISD(T)/cc-pVTZ value of the isomerization energy. To obtain a good value of the dissociation energy of $HONO_2$ to OH and NO_2, we combined our QCISD(T)/cc-pVDZ value of 104.0 kJ mol^{-1} for $\Delta U°$ (0 K) for the isomerization of $HONO_2$ to HOONO with Li and Francisco's value of 61.5 kJ mol^{-1} at the same level for $\Delta U°$ (0 K) for the dissociation of HOONO to OH and NO_2, obtaining an energy of dissociation of $HONO_2$ to OH and NO_2 of 165.5 kJ mol^{-1}. To obtain a better value we reoptimized a QCISD/cc-pVTZ structure for $HONO_2$, provided to us by Francisco (private communication), obtaining at the QCISD(T)/cc-pVTZ level a dissociation energy without zero-point corrections of 214.2 kJ mol^{-1} for $HONO_2$, which, combined with the QCISD(T)/cc-pVDZ ΔZPE value of −25.8 kJ mol^{-1}, yields a value of 188.4 kJ mol^{-1} for $\Delta U°$ (0 K), closer to the 197.3 kJ mol^{-1} value from experimental enthalpies of formation for $HONO_2$, NO, and NO_2,[44] for OH radical,[45,46] and for HO_2 radical[47] (also see ref 48).

Master Equation Methods

Since the reaction rates are energy dependent and collisional energy transfer involves weak collisions, the system is best treated using master equation techniques. To implement the master equation model, parameters must be assigned for three dissociation reactions and for energy transfer. In addition, rate constants for the reversible isomerization between *cis*- and *trans*-HOONO were also assigned. The numerous parameters were assigned by using conventional unimolecular reaction rate theory, the electronic structure calculations, and ancillary chemical kinetics data from the literature.

Rate Constant Expressions. In principle, each of the rate constants for dissociation and isomerization depends on vibrational energy and angular momentum, as does energy transfer. In the present work, a one-dimensional (vibrational energy) master equation treatment is employed with centrifugal corrections for angular momentum conservation. The centrifugal corrections are made using the pseudodiatomic approximation[49] and by assuming the energy in the "K-rotor" (conserved rotational degree of freedom) is limited only by the total active energy and mixes freely with energy that resides in the other active degrees of freedom. These approximations are both accurate and commonplace.[50] The MultiWell software package[51−53] was used for all of the calculations.

Unimolecular reaction rates were calculated using the RRKM theory,[49,50,54] which requires calculation of the sums and densities of internal states for the two potential wells and transition states. The electronic structure calculations provided normal mode vibrational frequencies and moments of inertia for the wells. In many cases, inspection of the normal mode motions enabled us to distinguish vibrational modes from the torsional modes, which were treated as hindered internal rotations. In the present work, all of the sums and densities of states are calculated (program DenSum[53]) by "exact counts" (energy grain of 10 cm^{-1}), using the Beyer−Swinehart algorithm[55] as adapted by Stein and Rabinovitch.[56]

According to RRKM theory,[49,50,54] the energy-dependent specific unimolecular rate constant $k(E)$ is given by

$$k(E) = \left[\frac{m^{\ddagger}}{m}\frac{\sigma_{ext}}{\sigma_{ext}{}^{\ddagger}}\right]\frac{g_e{}^{\ddagger}}{g_e}\frac{1}{h}\frac{G^{\ddagger}(E-E_0)}{\rho(E)} \qquad (2)$$

where $m^{\ddagger}$ and m are the number of optical isomers, $\sigma_{ext}{}^{\ddagger}$ and σ_{ext} are the external rotation symmetry numbers, and $g_e{}^{\ddagger}$ and g_e are the electronic state degeneracies of the transition state and reactant, respectively; h is Planck's constant, $G^{\ddagger}(E - E_0)$ is the sum of states of the transition state, E_0 is the reaction threshold energy, and $\rho(E)$ is the density of states of the reactant molecule. The internal energy E is measured relative to the zero-point energy of the reactant molecule and the reaction threshold energy (critical energy) is the difference between the zero-point energies of reactant and transition state. Equation 2 was written by assuming that the rotational *external* symmetry numbers, electronic degeneracies, and numbers of optical isomers were *not* used in calculating the sums and densities of states. It is, however, assumed that *internal* rotor symmetry numbers are used explicitly in the sum and density calculations and hence do not appear in eq 2. Note that the quantity set off in square brackets is the reaction path degeneracy.

Centrifugal corrections to the unimolecular rate constants were made according to the pseudodiatomic model, where the reaction threshold energy at a given temperature is corrected approximately for angular momentum effects by using a threshold energy $E_0{}^{T}$ given by the following expression[49]

$$E_0{}^{T} = E_0 - k_B T\left\{1 - \frac{I_{2D}}{I_{2D}{}^{\ddagger}}\right\} \qquad (3)$$

where I_{2D} and $I_{2D}{}^{\ddagger}$ are the moments of inertia for the external two-dimensional (2D) inactive (adiabatic) rotations of the reactant and of the transition state, respectively, and k_B is Boltzmann's constant. The resulting expression for $k(E)$ corresponds to that given by eq 4.31 in Robinson and Holbrook[54] or 3.31 in Holbrook et al.[57]

For a thermal distribution, recombination reaction rate constants (k_{rec}) are related to the corresponding unimolecular rate constants (k_{uni}) according to the equilibrium constant (K). Thus at the high-pressure limit we have the relationship

$$K = \frac{k_{\mathrm{rec}}^{\infty}}{k_{\mathrm{uni}}^{\infty}} \tag{4}$$

In the present work, equilibrium constants were calculated using the computer code Thermo,[53] which employs conventional statistical mechanics formulas for separable degrees of freedom that include harmonic and anharmonic oscillators, free and hindered internal rotors, and external rotational degrees of freedom.

In recombination reactions, the two reactants come together to form a highly excited adduct, which can redissociate, be collisionally deactivated, and react via other reaction channels. The chemical activation energy distribution[51] describes the nascent energy distribution of the complex formed in the recombination reaction

$$y_0^{(\mathrm{ca,i})}(E)\,\mathrm{d}E = \frac{k_{\mathrm{i}}(E)\rho(E)\mathrm{e}^{-E/k_{\mathrm{B}}T}\,\mathrm{d}E}{\int_{E_0}^{\infty} k_{\mathrm{i}}(E')\rho(E')\mathrm{e}^{-E'/k_{\mathrm{B}}T}}\,\mathrm{d}E', \text{ for } E \geq E_0 \tag{5}$$

where $y_0^{(\mathrm{ca,i})}(E)$ is the energy distribution of molecules formed via reaction channel i, which has energy threshold E_0 and specific rate constant $k_{\mathrm{i}}(E)$, $\rho(E)$ is the density of states in the new molecule, and the zero of energy for this equation is at the zero-point energy of the newly formed species.

Loose Transition States. For "loose" transition states, the properties of the transition state depend sensitively on angular momentum and the detailed shape of the interaction potential. In the absence of other information, it is possible to predict (to moderate accuracy) the rate constant by using variational transition-state theory or the statistical adiabatic channel model with a calculated high-accuracy potential energy surface.[50,58] When the rate constant is known, however, it is convenient to use a "restricted" Gorin model with a "hindrance parameter" selected to reproduce the known rate constant for the corresponding reverse (recombination) reaction.[50,59,60]

According to the Gorin model,[61] the two molecular fragments rotate independently of one another while separated at the distance corresponding to the centrifugal maximum (r_{max}) of the effective potential of the bond being broken. In the present work, the rotation of the OH radical was treated as a linear molecule, while those for NO_2 and the overall transition state were approximated as symmetric tops. The overall transition state has a 2D external adiabatic rotation with moment of inertia given by $I_{2\mathrm{D}}^{\ddagger} = \mu r^2_{\mathrm{max}}$, where μ is the reduced mass of the two fragments and a 1D external rotation (the "K-rotor") with moment of inertia I_{k}. The K-rotor is not adiabatic and is assumed, according to the usual approximation,[50] to mix energy freely with the active vibrations. The internal rotations of fragments A and B are characterized by 2D rotations with moments of inertia I_{a} and I_{b}, respectively, and an internal rotation with reduced moment of inertia I_{r}.

In the restricted Gorin model,[50,59,60] it is assumed that the two fragments interfere sterically with each another and thus cannot rotate freely. The effect is to reduce the available phase space and hence reduce the sum of states. Thus, the "transitional modes" have the characteristics of rotational degrees of freedom with heat capacity of $R/2$. Operationally, a "hindrance" parameter η is defined,[60] which can vary from zero (free rotation) to unity (completely hindered rotation). The 2D moments of inertia I_{a} and I_{b} are multiplied by the factor $(1 - \eta)^{1/2}$ to obtain the effective 2D moments of inertia used for calculating the sum of states. These parameters are listed in Table 5 for all of the restricted Gorin transition states used in the present work.

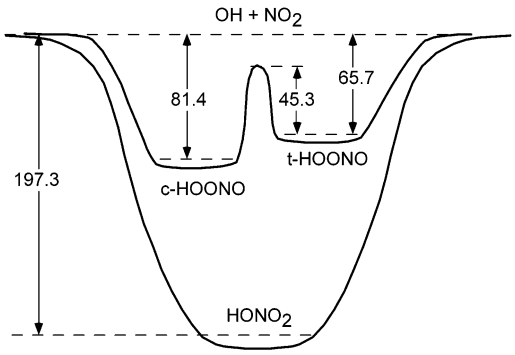

Figure 1. Schematic potential energy surface. Energies (kJ mol^{-1}): $HONO_2$ vs OH + NO_2 from experiments (see text for details); *cis*-HOONO vs *trans*-HOONO from ab initio results (this work); *cis*-HOONO vs OH + NO_2 from a reanalysis (this work, see Appendix) of experimental data.[4]

In general, the potential function describing the breaking bond is not known, but the Lennard-Jones potential is often chosen for its simplicity and because it has the long range dependence on r^{-6} expected for many long-range potentials. It does not describe a chemical bonding interaction very well at short range (near the potential minimum energy), however. For the Lennard-Jones potential, the moment of inertia for the two-dimensional adiabatic external rotation is given by $I_{2\mathrm{D}}^{\ddagger} = \mu r_{\mathrm{e}}^2(6D_{\mathrm{e}}/RT)^{1/3}$, where r_{e} is the equilibrium bond distance, μ is the reduced mass, and $D_{\mathrm{e}} = D_0 - \Delta E_{\mathrm{z}}$, where D_0 is the bond dissociation enthalpy at 0 K, ΔE_{z} is the zero point energy difference between products and reactants, and R is the gas law constant.

Energy Transfer Model. For present purposes, the conventional exponential-down model for the collision step size distribution is assumed

$$P(E,E') = \frac{1}{N(E')}\exp\left[\frac{-(E'-E)}{\alpha(E')}\right]$$
$$(E'-E) \geq 0 \tag{6}$$

where $P(E,E')$ is the probability density for energy transfer from vibrational energy E' to energy E in a deactivation step, $N(E')$ is a normalization factor, and the energy transfer parameter $\alpha(E')$ is approximately a linear function of internal energy and is almost identical to the average energy transferred in deactivating collisions (i.e., $\langle\Delta E\rangle_{\mathrm{down}}$). For single-channel reactions, it makes little quantitative difference in reaction simulations whether $\alpha(E')$ is treated as a constant, or as a function of energy. Although the present system involves several wells and multiple channels, little is known about energy transfer in this system and thus we minimized the number of adjustable parameters by assuming that $\alpha(E')$ is independent of energy and is the same for all wells. Collision frequencies were calculated by assuming Lennard-Jones intermolecular potentials (see Table 5 for parameters).

Models and Fitting to Experiments. According to the quantum chemical results described above, the combination of HO with NO_2 can lead to $HONO_2$ and at least two stable conformers of HOONO, as illustrated in Figure 1. The two HOONO conformers can interconvert via internal rotation about the interior O−N bond. Isomerization is possible between HOONO and $HONO_2$, presumably via the trans conformer of HOONO, but we have neglected this process for the following reasons. First, the lowest-energy transition state identified[40] for this process is ∼4 kJ mol^{-1} above the energy of OH + NO_2, the products of the O−O bond fission in HOONO. Second, the

TABLE 5: $HONO_2$, HOONO, and Transition State Properties

$HONO_2$	
critical energy at 0 K/kJ mol^{-1}	197.3
product of adiabatic moments of inertia/amu A^2	56.7
moment of inertia: active external rotor/amu A^2	42.1
collisions: (σ/A^2; ϵ/K; $\langle\Delta E\rangle_d$/cm^{-1}) $HONO_2$	4.3; 431
He	2.6; 10.2; 200
N_2	3.6; 91.5; 500
HO···NO_2 (Transition State)	
moment of inertia: active external rotor/amu A^2	39.1
product of adiabatic moments of inertia/ amu A^2: 430K; 300K; 250K; 220K	371.2; 418.9; 446.1; 465.2
hindrance: $(1 - \eta_a)^{1/2}$	0.50
HOONO	
critical energy at 0 K/kJ mol^{-1} (cis; trans)	81.4; 65.7
product of adiabatic moments of inertia/amu A^2 (cis; trans)	73.9; 107.6
moment of inertia: active external rotor/amu A^2 (cis; trans)	23.7; 9.75
collisions: (σ/A^2; ϵ/K; $\langle\Delta E\rangle_d$/cm^{-1}) $HONO_2$	4.3; 431; −
He	2.6; 10.2; 200
N_2	3.6; 91.5; 500
HO···ONO (Transition State)	
moment of inertia: active external rotor/amu A^2	16.5 (cis); 17.2 (trans)
product of adiabatic moments of inertia/ amu A^2, 430K; 300K; 250K; 220K	378.5; 421.8; 446.6; 465.0 (cis)
	456.6; 516.7; 549.2; 574.6 (trans)
hindrance: $(1 - \eta_b)^{1/2}$	0.35

transition state for the isomerization is expected to be "tighter" than that for the O−O bond fission, resulting in a smaller rate constant for HOONO molecules with the same internal energy.[16] Third, the precisely analogous RNO_3 systems have very small isomerization rates as the alkyl group (R) becomes smaller. In the limit of R = H, the measured isomerization rate is orders of magnitude smaller than the rate of O−O bond fission.[12,13,62−64] This is true in modeling studies, even when the isomerization barrier is assumed to be lower than that for O−O bond dissociation.[16] These considerations lead to the conclusion that isomerization between HOONO and $HONO_2$ can be neglected in the present system.

Even the limited system considered here requires multiwell, multichannel methods for calculation. Written as a reaction scheme, the system is comprised of the following reactions

$$OH + NO_2 \leftrightarrow HONO_2 \qquad (A,-A)$$

$$OH + NO_2 \leftrightarrow \textit{cis}\text{-HOONO} \qquad (B,-B)$$

$$OH + NO_2 \leftrightarrow \textit{trans}\text{-HOONO} \qquad (C,-C)$$

$$\textit{trans}\text{-HOONO} \leftrightarrow \textit{cis}\text{-HOONO} \qquad (D,-D)$$

The quantum chemical results give structural and vibrational frequencies of $HONO_2$ that are in good agreement with literature experimental values.[65] The ab initio vibrational frequencies correspond to the curvature at the bottom of the local minimum in the potential energy surface and do not include anharmonicity. Therefore, we assumed that the differences between the experimental vibrational frequencies ($v = 1$ to $v = 0$ transitions) are due solely to anharmonicity. The resulting $\omega_e x_e$ anharmonicity constants, which are presented in Table 6, are in fair agreement with those calculated for a Morse oscillator with the known bond dissociation energy. For example, a Morse potential corresponding to the O−H vibration frequency (3738 cm^{-1}) and bond dissociation energy (~450 kJ mol^{-1}) predicts an anharmonicity ($\omega_e x_e$) of −93 cm^{-1}, which is in excellent agreement with the corresponding value (−94 cm^{-1}) in Table 6. A Morse oscillator model for the HO−NO_2 bond (1786 cm^{-1} and 197.3 kJ mol^{-1}) predicts an anharmonicity of −48 cm^{-1}, which is in fair agreement with the value (−38 cm^{-1}) in Table 6. Since the actual bond potential energy is not exactly described by a Morse function, this level of agreement is satisfactory. Moreover, this procedure results in sums and densities of states that are similar to those obtained when using the measured transition frequencies. The values for x_e from $HONO_2$ were applied to the corresponding bonds in the HOONO species in order to obtain the corresponding $\omega_e x_e$ anharmonicity constants for the HOONO species (Table 6). The potential energy for hindered rotation around the O−N bond in $HONO_2$ was assumed to be 2-fold with reduced moment of inertia for rotation around the bond calculated using computer program MomInert.[51,53]

The HOONO species are connected to each other via internal rotations.[28] As discussed above, the cis−cis structure is the global minimum. Starting from the cis−cis structure, the hindered rotation around the O−O bond has a barrier that can be described as a sum of 1-fold and 3-fold components. The 1-fold component appears to be dominant, but the 3-fold component results in a rather narrow cis−cis potential well with a correspondingly high vibrational frequency. For present purposes, we neglected the 3-fold contribution and assumed a 1-fold NO−OH hindered internal rotation with a barrier of 1000 cm^{-1} and reduced mass for rotation around the bond. This assumption results in a lowered torsion frequency but a better representation of the internal rotation at high internal energies. In *trans*-HOONO (i.e., trans with respect to the ONOO moiety) the NO−OH internal rotation was assumed to have a symmetry number of two and was included explicitly in the density of states calculation. To avoid double counting of this effect in *trans*-HOONO, the number of optical isomers (m in Table 6) was set to unity. This is a somewhat confusing point, and the reader is referred to Gilbert and Smith[50] for a relevant discussion of optical isomers and symmetry numbers. The internal rotation around the OO−NO bond was treated as a 2-fold symmetric internal rotation with reduced moment of inertia for rotation about the bond. Thus the transition state for cis−trans isomerization via the OO−NO internal rotation corresponds to a perpendicular structure and hence two optical isomers.

TABLE 6: Molecular Constants[a]

	HO	NO_2	$HONO_2$	*cis*-HOONO	*trans*-HOONO
ΔU_f(0 K)	36.9	35.9	−124.5	−8.6	7.1
σ_e	1	2	1	1	1
g_e	4	2	1	1	1
m	1	1	1	1	1

HO				NO_2				$HONO_2$				*cis*-HOONO				*trans*-HOONO			
type	a	b	c	type	a	b	c	type	a	b	c	type	a	b	c	type	a	b	c
2-D		2-D		2-D				2-D				2-D				2-D			
rot	0.8914	rot		rot	39.748			rot	56.7			rot	73.9			rot	107.6		
K-rot		K-rot		K-rot	2.0861			K-rot	42.11			K-rot	23.7			K-rot	9.75		
vib	3737.76−84.88	1		vib	1318	0	1	hra	477	0.882		hrc	0.915	1000	1	vib	205.5	0	1
				vib	749.65	0	1	vib	576	0	1	vib	397	0	1	hra	293.4	0.913	2
				vib	1617.8	0	1	vib	644	0	1	vib	515	0	1	vib	353.2	0	1
								vib	762	0	1	vib	618	0	1	vib	442.4	0	1
								vib	892	−6	1	vib	796	−8	1	vib	773.7	−7.7	1
								vib	1337	−16	1	vib	939	−9.4	1	vib	950.8	−0.5	1
								vib	1360	−17	1	vib	1461	−14.6	1	vib	1392.2	−13.9	1
								vib	1786	−38	1	vib	1649	−21.4	1	vib	1758.5	−22.9	1
								vib	3738	−94	1	vib	3496	−83.9	1	vib	3753.2	−90.1	1

[a] ΔU_f(0 K), internal energy of formation at 0 K (kJ/mol); σ_e, external symmetry number; g_e, electronic degeneracy; m, number of optical isomers. Type: 2-D rot, 2-D external (adiabatic) rotation; K-rot, 1-D external (active) rotation; vib, vibration; hra, hindered rotor, given vibrational frequency and moment of inertia; hrc, hindered rotor, given moment of inertia and hindrance barrier height. Columns: moment of inertia (rot, hra, amu Å^2) or frequency (vib, cm^{-1}); moment of inertia (hrc, amu Å^2) or anharmonicity (vib, cm^{-1}); degeneracy (vibs) or symmetry (rots and hindered rotors).

TABLE 7: Calculation of Moments of Inertia

T	LJ max[a]	$r + r_\Delta$[b]	$r^\# + r_\Delta$[c]	$r^\#$[d,e]	I_a	I_b	I_c	K-rot	$(I_b \cdot I_c)^{1/2}$
				cis-HOONO, $D_e = 19.6$, $r = 1.422$					
					58.91	83.64	24.73	24.73	70.20
300	2.41	2.38	5.74	4.78	16.53	430.15	413.62	16.53	421.80
250	2.49	2.38	5.91	4.96	16.74	455.05	438.31	16.74	446.60
220	2.54	2.38	6.04	5.09	16.88	473.53	456.65	16.88	465.01
430	2.27	2.38	5.40	4.45	16.11	370.57	386.68	16.11	378.54
				trans-HOONO, $D_e = 17.7$, $r = 1.422$					
					9.38	102.70	110.39	9.38	106.47
300	2.37	2.93	6.95	5.44	17.24	525.38	508.14	17.24	516.69
250	2.45	2.93	7.16	5.66	17.44	557.95	540.51	17.44	549.16
220	2.50	2.93	7.32	5.81	17.58	583.50	565.92	17.58	574.64
430	2.23	2.93	6.54	5.04	16.82	448.25	465.01	16.82	456.55
				$HONO_2$, $D_e = 47.16$, $r = 1.422$					
					38.45	80.62	42.17	38.45	58.31
300	2.79	2.17	6.05	5.29	39.05	438.92	399.87	39.05	418.94
250	2.88	2.17	6.24	5.48	39.05	466.05	427.00	39.05	446.10
220	2.94	2.17	6.37	5.61	39.05	485.14	446.09	39.05	465.20
430	2.63	2.17	5.70	4.94	39.05	391.27	352.23	39.05	371.24

[a] LJ Max $= (6D_e/RT)^{1/6} = (r^\# + r_\Delta)/(r + r_\Delta)$. [b] $r + r_\Delta =$ (J(molecule)/(reduced mass))$^{1/2}$. [c] $r^\# + r_\Delta = (r + r_\Delta)$*X. [d] $r^\# = (r^\# + r_\Delta) - (r + r_\Delta) + r$. [e] The values of $r^\#$ are used in computing moments of inertia in the transition states.

Energies of formation of OH, NO_2, and $HONO_2$ leads to ΔU/kJ mol^{-1} = 197.3. The analysis in the Appendix leads to ΔU/kJ mol^{-1} = 81.4 and 65.7 for cis−cis and trans−perp, respectively. It is important to note that although we employ values for ΔU to three significant digits, the actual values are certainly known to no better than ±4 kJ mol^{-1}, which can lead to errors in the equilibrium and rate constants as large as a factor of ×10 at 220 K. Even small differences in the literature for values of structure and frequencies give rise to errors in the equilibrium constant for $HONO_2$ formation from HO and NO_2 that are at least ±20%!

The assumption of a 1-fold internal rotation around the O−O bond in *cis*-HOONO (discussed above) produces a slightly higher entropy than if a 3-fold hindered rotor is assumed. It is difficult to make a quantitative estimate of the effect on the enthalpies deduced from a third-law analysis of measurements (see Appendix), but we estimate the effect is ≤2 kJ mol^{-1}. Equilibrium constants based on these considerations are presented in Table 8.

The properties of the transition state for reaction D are given in Table 3. Because the two reaction paths are almost identical, we adopted the vibrational frequencies and structure of one transition state and assumed the second path is identical. The calculated A factors of 1.3×10^{13} s^{-1} and 8.5×10^{12} s^{-1} for reactions D and −D, respectively, appear to be reasonable in comparison with other reactions.[59]

The loose transition states were treated as hindered Gorin species in the manner of Golden and Smith.[7] The centrifugal correction is made in the usual way,[49,50,54,57] by correcting the energy variable in the RRKM calculation to take into account the conservation of angular momentum. This in turn requires a value for the moment of inertia of the psuedodiatomic molecules representing the reactant and the transition state. This quantity is determined by computing the moments of inertia of the

TABLE 8: Equilibrium Constants and Recombination Rate Constants (High-Pressure Limit)

	$OH + NO_2 \leftrightarrow HONO_2$		$OH + NO_2 \leftrightarrow$ *cis*-HOONO		$OH + NO_2 \leftrightarrow$ *trans*-HOONO	
T (K)	K_{eq}[a]	$k_{rec,\infty}$[b]	K_{eq}[a]	$k_{rec,\infty}$[b]	K_{eq}[a]	$k_{rec,\infty}$[b]
220	5.58 (20)	2.74	3.05 (−7)	1.57	1.01 (−10)	3.82
250	1.02 (15)	2.73	1.24 (−9)	1.57	1.19 (−12)	3.79
300	9.72 (7)	2.72	1.50 (−12)	1.57	5.28 (−15)	3.77
430	2.31 (−3)	2.75	6.21 (−17)	1.62	1.64 (−18)	3.80

[a] Notation: 5.58 (20) = 5.58×10^{20}. Units: cm^3 $molecule^{-1}$. [b] Units: 10^{-11} cm^3 s^{-1}.

reactant and the transition state, assuming that the smallest moment is the active "K-rotor" and using the root-mean-square of the other two moments as the 2D moment of the pseudodiatomic molecule. The calculation of the moments of inertia of the transition state requires geometric parameters. All the parameters of either $HONO_2$ or the appropriate HOONO molecule are used, except that the HO−NO_2 or HO−ONO distances are determined from an assumption about the potential energy of interaction between the HO and NO_2. Golden and Smith[7] used a Lennard-Jones potential. In this work we use a modification of the model used by Golden and Smith. The modification is to compute the maximum value of the interaction along a coordinate defined by the bond distance between the O in the OH moiety and the N in the NO_2 for $HONO_2$ or the O in NO_2 for the HOONO cases plus a quantity r_Δ. This last quantity is defined by taking the pseudodiatomic moment of the molecule, as defined above, and setting it equal to the reduced mass multiplied by a distance squared. That distance is defined as r_Δ added to r_e (the value of the bond distance at equilibrium). Table 7 contains the calculations of moments of inertia. This arbitrary definition simply affects the magnitudes of α needed to fit the data. Thus, *quantitative knowledge of these parameters is too vague to permit precise calculation of the rate constant at the low-pressure limit from known molecular properties*. If Morse or Varshni potentials are used, the 2D moments of inertia are different, resulting in different values of α needed to fit the experimental data.[16]

The amount of hindrance (η) was used as a fitted parameter to match the experimental $HONO_2$ formation rate constants at 430 K and 130 bar from Hippler et al.,[4] which are near the high-pressure limit. According to the hindered Gorin model, moments of inertia of the 2D rotors of OH and of NO_2 were each multiplied by the quantity $(1 - \eta_i)^{1/2}$ for the ith species.[7,59,60] A very good fit was obtained for $HONO_2$ with $(1 - \eta_a)^{1/2} = 0.50$ (i.e., $\eta_a = 0.75$), as shown in Figure 2. Under the same conditions, the rate constants for HOONO formation are not as close to the high-pressure limit and are hence not very sensitive to the value of the hindrance; they are much more sensitive to the assumed energy transfer parameters.

A satisfactory fit to the HOONO formation rate constants at 430 K (Figure 2) and the OH radical loss rate constants at 300 K (Figure 3) in helium were obtained by using $(1 - \eta_a)^{1/2} = 0.50$ for $HONO_2$, $(1 - \eta_b)^{1/2} = 0.35$ for HOONO, and energy transfer parameter $\alpha_{He} = 200$ cm^{-1} for both $HONO_2$ and the HOONO species (all values of α are assumed to be independent of temperature[66] and internal energy). An even better fit of both data sets could be obtained by using $\alpha_{He} = 175$ cm^{-1} for $HONO_2$ and $\alpha_{He} = 250$ cm^{-1} for the HOONO species, but when just one value of the parameter was used, $\alpha_{He} = 200$ cm^{-1} was found to be a good compromise. It was only possible to distinguish the apparent differences in α because data in helium collider gas are available for pressures ≥100 bar at both temperatures. Such high-pressure data are not available for N_2 collider gas, and thus we decided to use the single value of α for all of the HNO_3 isomers.

Because the use of the hindered Gorin model is arbitrary and η_a and η_b are simply used as fitting functions, we do not assign any physical significance to their differences. For convenience, the values for η_a and η_b were assumed to be independent of temperature. The resulting high-pressure limiting rate constants for $OH + NO_2$ to form either $HONO_2$ or HOONO are nearly independent of temperature, in agreement with conclusions reached by Troe[19] and by Maergoiz et al.[67,68] Thus it is assumed for convenience that both the energy-transfer parameters (α_i) and the hindrance parameters (η_i) are independent of temperature. Other assumptions could be made, but they would require additional parameters. In particular, if the hindrance parameters are assumed to be larger at higher temperatures, due to shifts in the centrifugal barriers, then the energy transfer parameters would have to be made temperature-dependent as well. Alternatively, one could also assume that the formation of *cis*-HOONO and *trans*-HOONO proceed through a common transition state and the result would likely still be consistent with the experimental data.

The recombination rate constant is obtained from the equilibrium constant and the decomposition rate constant, which is calculated according to RRKM Theory. For reaction A, for example, $k_A = k_{-A}K_A$, where the rate constants are written in lower case and the equilibrium constant is written in upper case. Equilibrium constants and the corresponding recombination rate constants (high-pressure limit) for the models described here are presented in Table 8. The results are in good accord with other estimates of the high-pressure limit for this reaction system.[7,17−19]

Three sets of 10^6 stochastic trials were carried out using MultiWell for each temperature and pressure. The first set was for simulating formation of excited $HONO_2$ via reaction A. The excited species can either dissociate via reaction −A or be collisionally stabilized. Depending on temperature and the identity of the value of the energy transfer parameter α, between 15 and 100 collisions were needed to stabilize the excited species. The results of the calculation are in the form of the fractional yield of thermalized $HONO_2$. When multiplied by the high-pressure limit recombination rate constant, the fractional yield gives the falloff value for the recombination rate constant to produce $HONO_2$. The second and third sets of stochastic trials were for simulating formation of excited *cis*- and *trans*-HOONO via reactions B and C, respectively. The excited HOONO species can undergo isomerization via reactions D and −D, decomposition via reactions −B and −C, or collisional stabilization. Each of these sets of stochastic trials predicted that both HOONO conformers are formed in yields that vary as functions of temperature and pressure. By multiplying the fractional yields by the high-pressure limit recombination rate constant, one can calculate the falloff rate constant for producing a specific product via a recombination reaction. The rate constants calculated in this way for the two HOONO recombination reactions were summed appropriately to obtain the rate constants discussed below.

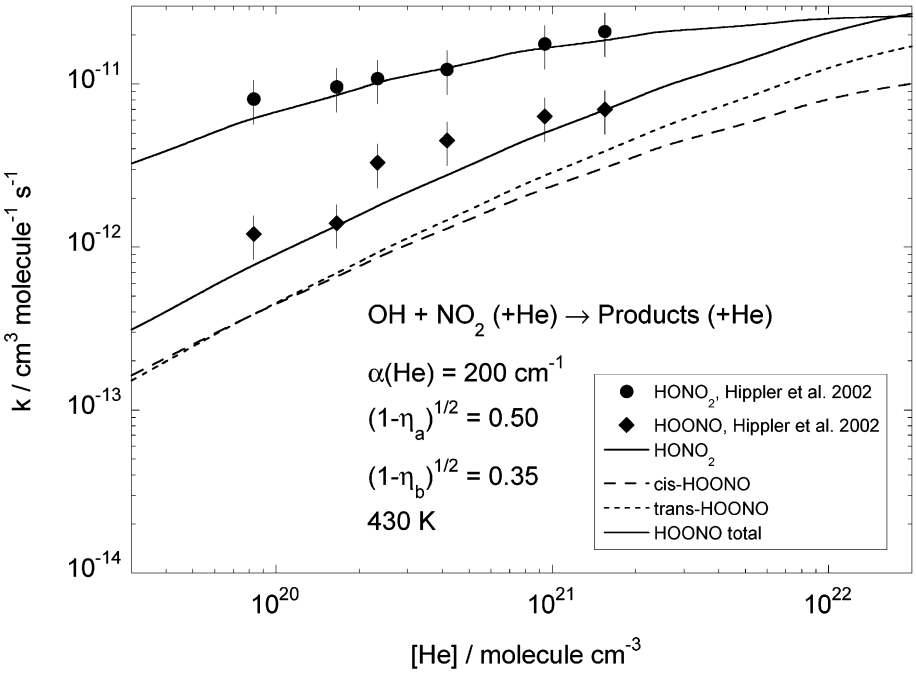

Figure 2. Data for the rate constant for $HONO_2$ and HOONO formation at 430 K in helium buffer gas from Hippler et al.[4] The lines are the interpolated results of master equation calculations for $HONO_2$ formation and for formation of the indicated HOONO species, calculated using the parameters in Table 5.

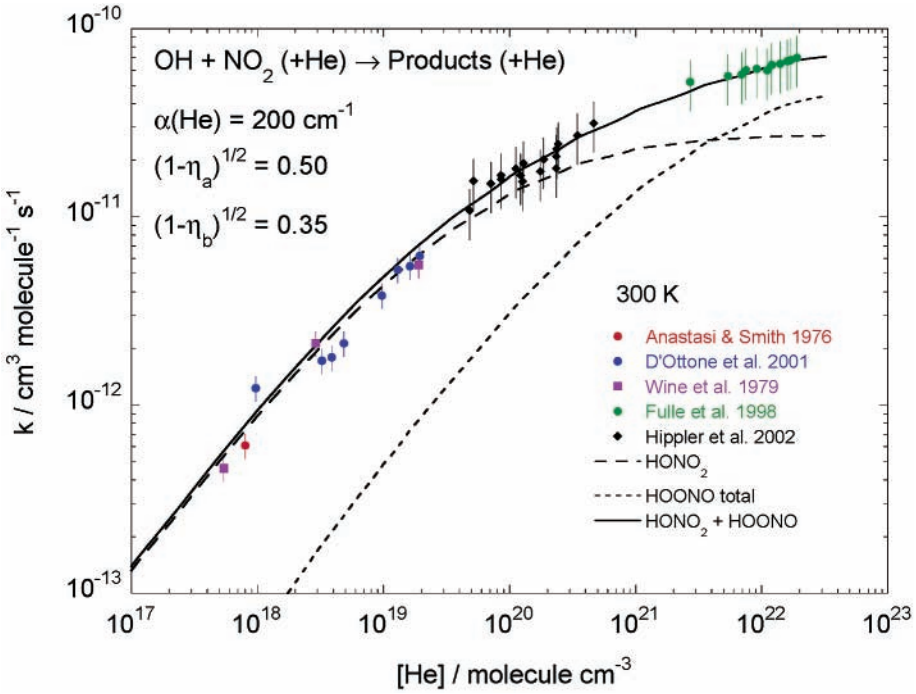

Figure 3. Data for the rate constant for the reaction between HO and NO_2 at 300 K in helium buffer gas, from various sources,[4,20,23,24,26] as indicated in the figure legend. The lines are the interpolated results of master equation calculations for $HONO_2$ formation and for formation of the indicated HOONO species, calculated using the parameters in Table 5.

Results and Discussion

Experimental data and computed rate constants are compared in Figures 2−6. Figure 2 shows the data of Hippler et al.[4] for formation of what they ascribe to HOONO and $HONO_2$ in helium bath gas. The $HONO_2$ data are well described by the model with $(1 - \eta_a)^{1/2} = 0.50$ and with energy transfer parameter $\alpha = 200$ cm^{-1}. The HOONO data are reasonably well described by summing the separately calculated rate constants for the two isomers, both with $(1 - \eta_b)^{1/2} = 0.35$ and with $\alpha = 200$ cm^{-1}. As mentioned above, even better agreement with the data can be obtained by lowering α to 175 cm^{-1} for $HONO_2$ and raising it to 250 cm^{-1} for HOONO. This difference is qualitatively in agreement with the notion that internal rotations and lower vibrational frequencies result in energy transfer that is more efficient; the lowest frequencies in HOONO are lower than those in $HONO_2$, and HOONO contains two internal rotations, in contrast to the single internal rotation found in $HONO_2$. Although reasonable, the magnitudes of α depend on the specific transition-state models and do not necessarily

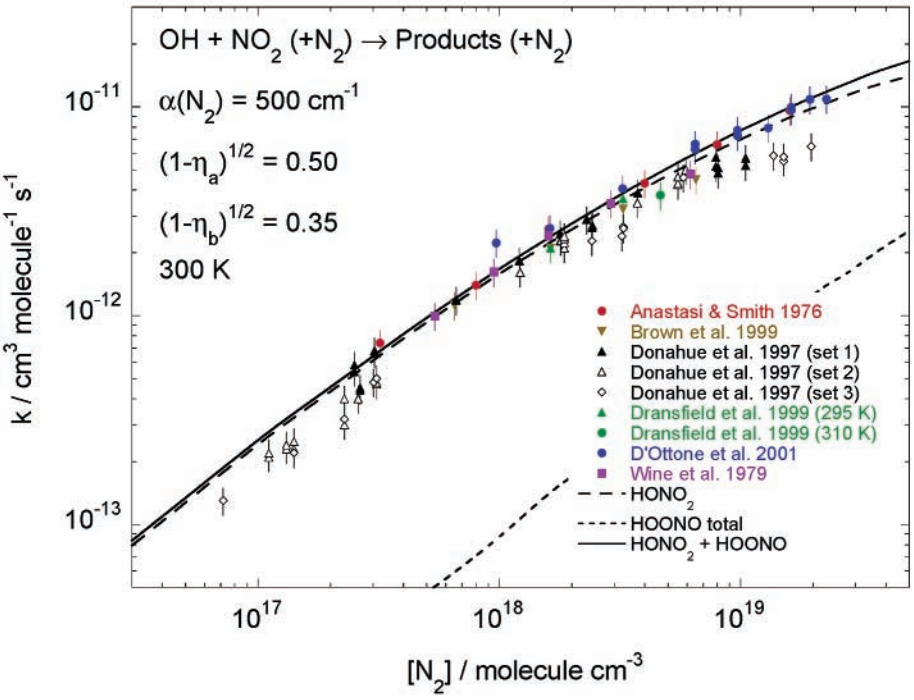

Figure 4. Data for the rate constant for the reaction between HO and NO_2 at 300 K in helium buffer gas, from various sources,[20−23,25,26] as indicated in the figure legend. The lines are the interpolated results of master equation calculations for $HONO_2$ formation and for formation of the indicated HOONO species, calculated using the parameters in Table 5.

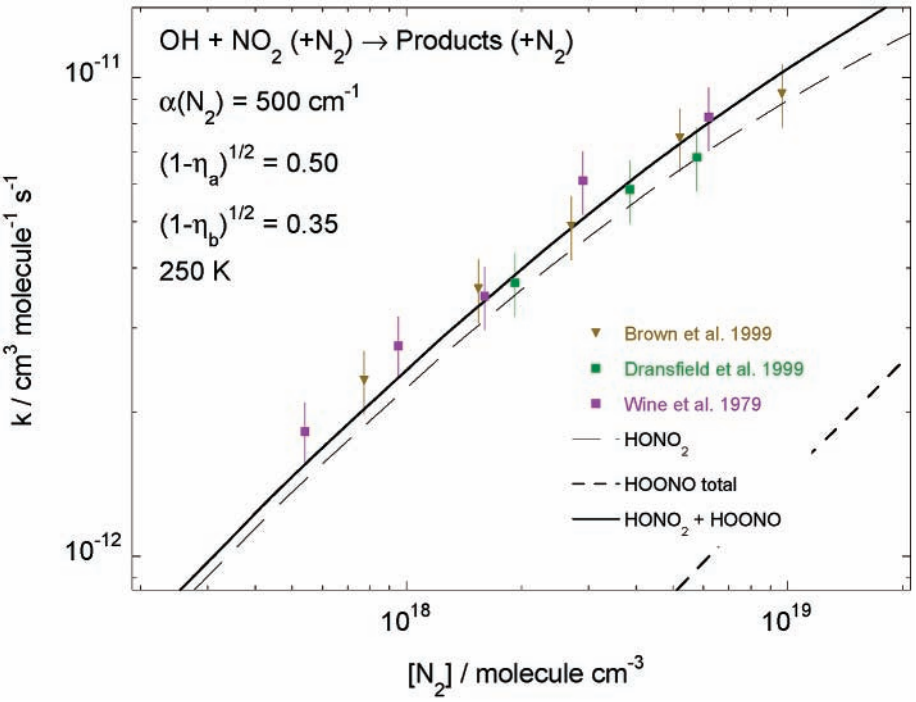

Figure 5. Data for the rate constant for the reaction between HO and NO_2 at 250 K in N_2 buffer gas, from various sources,[21−23] as indicated in the figure legend. The lines are the interpolated results of master equation calculations for $HONO_2$ formation and for formation of the indicated HOONO species, calculated using the parameters in Table 5.

equal the values that would be obtained in direct energy transfer measurements.[66]

Figures 3 and 4 present data at 300 K in He and N_2, respectively, along with calculated values of the rate constants as a function of number density. It is only in the very high-pressure He data that the effect of the HOONO pathway becomes apparent at 300 K. In contrast to He collider gas, it is not possible to determine separate energy parameters for $HONO_2$ and HOONO in N_2 collider gas, since super-high-pressure data are not available. Figures 5 and 6 show data in N_2 at 250 and 220 K, respectively, together with rate constants from the master equation calculations. All in all, the comparisons are consistent with the assumption that the high-pressure limit recombination rate constant and the energy-transfer parameter are essentially independent of temperature.

This comprehensive master equation model for the $HONO_2$/HOONO system can be used to estimate detailed information that has not yet been measured. For example, the yields of

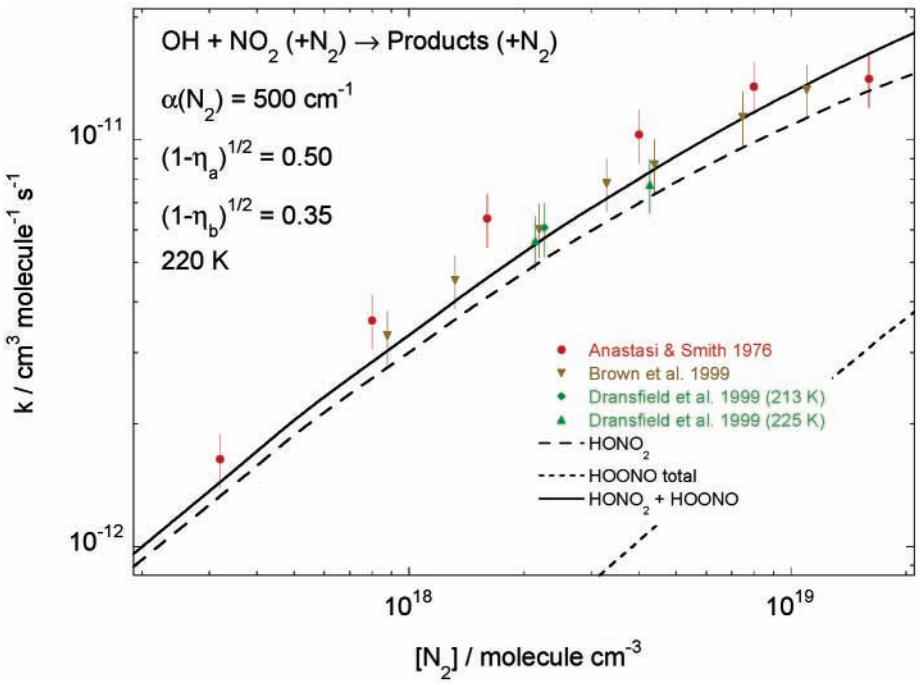

Figure 6. Data for the rate constant for the reaction between HO and NO_2 at 220 K in N_2 buffer gas, from various sources,[20−22] as indicated in the figure legend. The lines are the interpolated results of master equation calculations for $HONO_2$ formation and for formation of the indicated HOONO species, calculated using the parameters in Table 5.

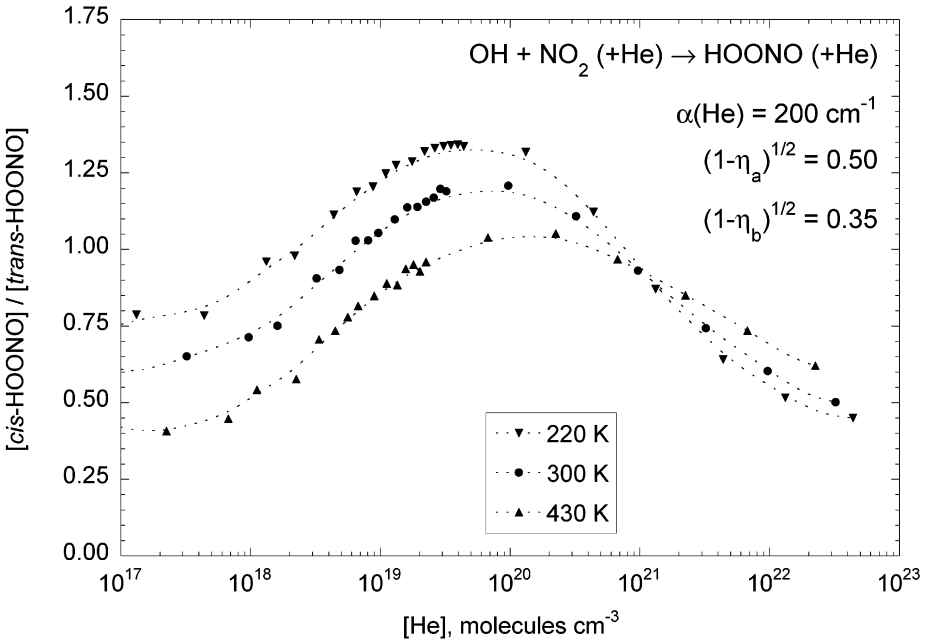

Figure 7. Relative rates of formation of the *cis*- and *trans*-HOONO conformers in helium buffer gas, calculated using the parameters in Table 5. (The dotted lines are merely to guide the eye.)

$HONO_2$ and HOONO are indicated in Figures 2−6. Also, the ratio of the rate constants for production of *cis*-HOONO vs *trans*-HOONO conformers is predicted to reach a maximum at intermediate pressures, which vary as a function of temperature, as shown in Figure 7. Such ratios will be important if the physical and chemical properties of the two conformers differ sufficiently to be significant in chemical systems such as the atmosphere.

Fitting the Results to Semiempirical Functions. It has been the practice in both the atmospheric and combustion communities to represent unimolecular reactions (and their reverse) using the methods put forth by Troe.[69,70] Convenient analytical expressions are obtained with the following form

$$k(M,T) = \left\{\frac{k_0(T)[M]}{1 + (k_0(T)[M]/k_\infty(T))}\right\}F \qquad (7)$$

The term in braces is derived from the Lindemann−Hinshelwood mechanism[71] and the factor F takes into account the fact that the energy dependence of the specific rate constant is more complicated than that assumed by Lindemann−Hinshelwood, leading to a "broadening" of the curve. Troe further suggested that the "broadening factor," F, could be written as F_c^x, where

TABLE 9: Fitted Parameters

	$k_0'(T) = k_0^{300}(T/300)^{-n}$		$k_\infty(T) = k_\infty^{300}(T/300)^{-m}$		$F_c(T) = F_c^{300}(T/300)^{-q}$		$J(T) = J^{300}(T/300)^{-r}$	
	k_0^{300}	n	k_∞^{300}	m	F_c^{300}	q	J^{300}	r
				NASA[a]				
$HONO_2$	1.8 (−30)	3.0	2.8 (−11)	0	0.6			
HOONO (sum)	9.1 (−32)	3.9	4.2 (−11)	0.5	0.6			
				IUPAC[b]				
$HONO_2$	1.9 (−30)	2.0	2.8 (−11)	0	0.60	0.5		
HOONO (sum)	1.1 (−31)	4.1	6.1 (−11)	0.1	0.34	0.3		
				J equation[c]				
$HONO_2$	2.3 (−30)	3.0	2.7 (−11)	0			6.8	0
HOONO (sum)	1.1 (−31)	3.1	6.9 (−11)	−0.8			24.8	−3.5
cis-HOONO	4.9 (−32)	3.6	1.6 (−11)	0			5.0	0.1
trans-HOONO	3.1 (−32)	4.4	3.8 (−11)	0			5.6	−0.4

[a] Equation 8. [b] Equation 9. [c] Equation 10.

TABLE 10: Third Law Heat of Formation for *cis*−*cis*-HOONO

T (K)	K_{eq} (bar^{-1})	factor	$K_{cis-cis}$ (bar^{-1})	ΔG(expt) (kJ mol^{-1})	ΔS(rxn) (J mol^{-1} K^{-1})	$\Delta H = \Delta G + T\Delta S$ (kJ mol^{-1})	$\Delta(H(T) - H(0))$ (kJ mol^{-1})	ΔH(0 K) (kJ mol^{-1})
430	670	1.03	653	−23.17	−142.5	−84.45	−4.75	−79.70
435	650	1.03	632	−23.33	−142.5	−85.31	−4.73	−80.58
440	520	1.03	505	−22.77	−142.5	−85.47	−4.71	−80.76
443	510	1.03	495	−22.85	−142.4	−85.94	−4.70	−81.24
445	450	1.03	437	−22.49	−142.4	−85.86	−4.70	−81.16
448	510	1.03	494	−23.10	−142.4	−86.90	−4.69	−82.21
450	340	1.03	329	−21.69	−142.4	−85.77	−4.68	−81.09
455	280	1.03	271	−21.19	−142.3	−85.94	−4.66	−81.28
460	240	1.04	232	−20.83	−142.3	−86.28	−4.64	−81.64
465	220	1.04	212	−20.71	−142.2	−86.83	−4.62	−82.21
470	190	1.04	183	−20.35	−142.2	−87.19	−4.60	−82.59
475	140	1.04	134	−19.36	−142.2	−86.90	−4.57	−82.33
							average =	−81.40
							ΔH_f(HOONO)	−8.60

the factor "F_c" is the broadening correction at the center of the falloff curve (i.e., when $k_0(T)[M] = k_\infty(T)$) and the quantity x is some function of the rate parameters and the pressure.

In the atmospheric chemistry community, two compilations of rate data are widely used, one due to NASA[1] and the other to IUPAC.[2] These groups have used somewhat different versions of the Troe expression. According to the NASA format, the rate constant has been written

$$k(M,T) = \left\{\frac{k_0(T)[M]}{1 + (k_0(T)[M]/k_\infty(T))}\right\} 0.6^{\{1+[\log(k_0(T)[M]/k_\infty(T))]^2\}^{-1}} \quad (8)$$

In contrast, the IUPAC format is written

$$k(M,T) = \left\{\frac{k_0(T)[M]}{1 + (k_0(T)[M]/k_\infty(T))}\right\} F_c^{\{1+[\log(k_0(T)[M]/k_\infty(T))/(0.75-1.27\log(F_c))]^2\}^{-1}} \quad (9)$$

There are two obvious differences between these formulations. First, the NASA formulation assumes that $F_c = 0.6$ is a constant under atmospheric conditions (typically $200 < T/K < 300$ and $1 < P/Torr < 760$), while the IUPAC formulation adopts different values for F_c for each reaction. (This introduces an additional parameter into the formulations as written, but the IUPAC group often suggests that k_∞ is not temperature dependent, thus reducing the number of parameters.) Second, the IUPAC formulation takes into account the asymmetry expected in the falloff curve, although the term $(0.75-1.27 \log F_c)$ is very close to unity when $F_c = 0.6$, as assumed in the NASA formulation and often suggested in the IUPAC recommendations.

A third representation of falloff data is Oref 's J equation,[72] which is based on RRKM theory

$$k(M) = \{-(k_\infty + k_0) + [(k_\infty + k_0)^2 + 4(J-1)k_\infty k_0]^{1/2}\}[2(J-1)]^{-1} \quad (10)$$

Like the IUPAC representation, the J equation requires three temperature-dependent parameters. Hessler and Ogren commented[73] that the J equation gives less correlation among fitted parameters than do the Troe formulas when used for fitting data on the $CH_3 + CH_3$ recombination reaction.

If accurate and exceptionally precise data exists for any given process, the above formulations could be compared and the best representation identified, as has been attempted recently by several authors.[72−79] Furthermore, various possible protocols for fitting the results could be evaluated. The data for reaction 1, however, are not precise enough for such a determination, which is one reason we carried out the master equation calculations. Nonetheless, the above formulations are useful and even necessary for practical interpolation of the master equation results. Thus we have fitted the master equation results to each of the three formulations described above by making no prior assumptions about the magnitudes of the low- and high-pressure limiting rate constants. In each case, we have assumed that the

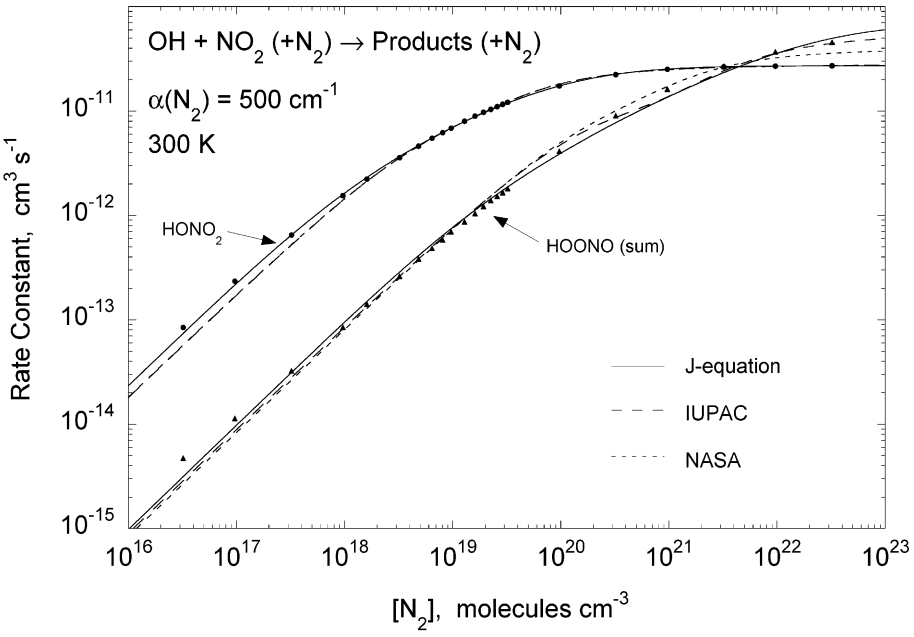

Figure 8. Nonlinear least-squares fits of master equation results by three semiempirical functions: the NASA two-parameter function (eq 8), the IUPAC function (eq 9), and the J Equation (eq 10).

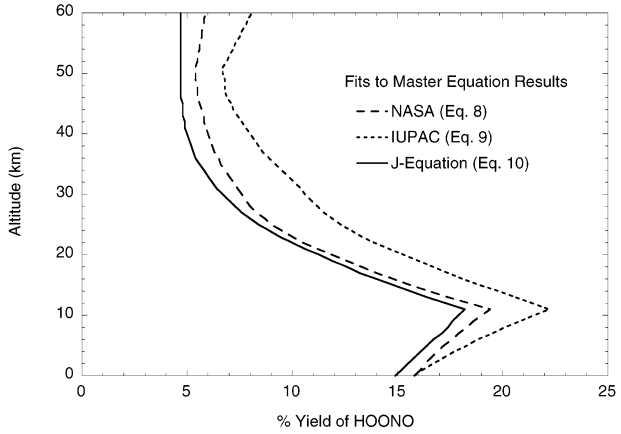

Figure 9. Predicted relative yield of HOONO as a percentage of the total rate of the OH + NO_2 reaction as a function of altitude, based on the U.S. Standard Atmosphere, 1976.[88,89]

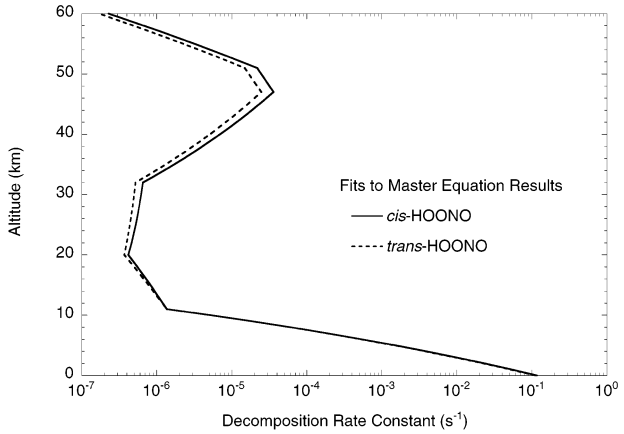

Figure 10. Predicted rate constants for thermal decomposition of *cis*- and *trans*-HOONO as a function of altitude, based on the U.S. Standard Atmosphere, 1976.[88,89]

parameters k_0, k_∞, F_c, and J may be temperature dependent according to the following empirical expression

$$X(T) = X_{300}\left[\frac{T}{300}\right]^{-a} \qquad (11)$$

where $X(T)$ and X_{300} are the values of k_0, k_∞, F_c, or J at T and at 300 K, respectively, and a is a parameter.

The results of the fits are presented in Table 9 and representative fits are presented in Figure 8. The fitting was carried out using the Levenburg−Marquardt algorithm[80,81] for nonlinear least-squares analysis as implemented by KaleidaGraph software.[82] Fits included pressures from 0.3 to 10^6 Torr, inclusive, and were weighted for $HONO_2$ according to the stochastic uncertainties calculated by MultiWell[51,53] and for HOONO according to the sum of the rate constants for the two species. The weighting for HOONO amounts to assuming a log-normal error distribution with constant relative error. Note that in the version of MultiWell employed in these calculations, a minor artifact caused the master equation results at k/k_∞ less than ~0.001 to deviate slightly from the expected linear asymptotic behavior. Tests showed that this deviation did not significantly affect the fits to the three semiempirical functions.

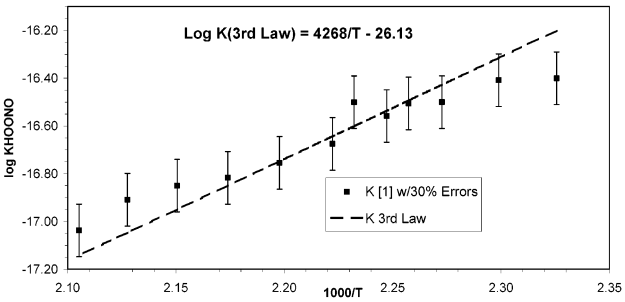

Figure 11. Third-law fit to K/cm^3 molecule^{-1} for HOONO formation.

The results presented in Figure 8 show that although the Oref *J* equation tends to fit the results slightly better than the other functions over the entire pressure range, all of the fits are of comparable accuracy. Note that the HOONO master equation results are the sum of the results obtained separately for the cis and trans forms. The semiempirical fits are not as good for the HOONO sum, but they are still generally adequate. Note that

other fitting protocols will lead to slightly different sets of parameters and one or another of the three semiempirical representations might emerge as slightly better than the other two, but considering the differences among the experimental data reported by various laboratories (e.g., Figure 4), any of the three choices will give satisfactory results. The only significant differences that emerge are in atmospheric chemistry models that explicitly include HOONO at altitudes above the stratopause, where the yields of $HONO_2$ and HOONO are, however, very small (see below).

Atmospheric Implications. Reaction 1a is a key chain termination step throughout the lower atmosphere. The formation of HOONO via reaction 1b is likely to have an effect because it is highly unlikely that HOONO is as stable as $HONO_2$, which is long-lived. In the troposphere, if HOONO dissolves in cloudwater or aerosol particles, the subsequent aqueous photochemistry is likely to be similar to H_2O_2(aq),[83,84] rather than to $HONO_2$(aq), which is more stable photochemically.[85−87] In the stratosphere, HOONO may photolyze or react with free radicals relatively rapidly, but the rate constants and mechanisms are not known.

The fractional yield of HOONO is presented in Figure 9 as a function of altitude, according to the three semiempirical fitting functions discussed above and the 1976 US Standard Atmosphere.[88,89] The results show that the yield of HOONO is a maximum near the tropopause, where the temperature is lowest and the pressure is still relatively high. At altitudes below about 50 km (the top of the stratosphere), the three functions are in reasonable agreement, but at higher altitudes, the three fits diverge from each other. At the low pressure limit, the fractional yield of HOONO is expected to become essentially constant, more like the fit to Oref's *J* equation, which produces fits that are slightly better than the other two functions, as discussed above. This divergence at altitudes above 50 km is not very significant, however, because the reactions are near the low-pressure limit and the rates of production of both $HONO_2$ and HOONO are relatively small.

Rate constants for decomposition of *cis*- and *trans*-HOONO are presented in Figure 10 as a function of altitude, based on fits to Oref's *J* equation (see Table 9). These rate constants can be used to estimate the lifetime of HOONO with respect to thermal decomposition. The actual atmospheric fate of HOONO at altitudes near and above the tropopause may, however, depend more on the currently unknown rates of photolysis and reaction with ambient free radicals.[7]

Conclusion

The multiwell, multichannel master equation model is in very good agreement with all of the experimental kinetics data. The data at 300 K with He pressures of the order of 10 bar or greater clearly shows some effect of a second HNO_3 isomer as do the data of Hippler et al.[4] near 430 K, which exhibit a double exponential decay of OH and clearly suggest the formation of more than one isomer. At least one HOONO isomer product of the reaction has been identified spectroscopically by Nizkorodov et al.[9]

Although there is little doubt that the species HOONO is formed along with $HONO_2$ in the interaction of HO with NO_2, the model suggests that a maximum of ∼20% of HOONO is formed near the tropopause. It is difficult to confirm this within the combined uncertainty of the data and the model. Fits of the master equation results to semiempirical models produce practical representations that are useful of atmospheric chemistry models.

Even better understanding of these reactions can be achieved through experimental measurements of the HOONO isomer branching ratios over a wide range of pressures and temperatures. Measurements of the rate constants under N_2 pressures greater than 10 bar at low temperatures will also be very helpful in refining the model.

Acknowledgment. D.M.G. has been supported by the NASA Upper Atmosphere Research Program through Grant NAG-2-1397-1 to Stanford University. J.R.B. thanks NSF, Atmospheric Chemistry Division, for partial support. This work was stimulated by a month in Horst Hippler's Laboratory at the University of Karlsruhe supported by Sonderforschungsbereich 551. As always, discussions with Gregory P. Smith are helpful and stimulating. Thanks also go to Barney Ellison and Joe Francisco for sharing results prior to publication and for discussions. Thanks go to Sheo Prasad for suggesting the view offered in Figure 9. (This material is based upon work supported by the National Science Foundation under Grant No. 9812680. Any opinions, findings, and conclusions or recommendations expressed in this material are those of the authors and do not necessarily reflect the views of the National Science Foundation.)

Appendix: Thermochemistry of HO + NO_2 = HOONO

Theoretical studies allow the calculation of equilibrium constants for the formation of each of the conformers of HOONO. As discussed in the text, recent high level calculations, including the one herein, conclude that the cis−perp structure is essentially unstable and should not be included in any equilibrium calculations. Frequencies and structures for all conformers and transition states between them are given in Table 5. Relative values for ΔU/kJ mol^{-1} employed herein, from QCISD(T)/cc-pVDZ calculations, were 0.0 and 15.7 for cis−cis and trans−perp, respectively. Using these values, ratios of the individual equilibrium constants can be computed, assuming the *cis*- and *trans*-HOONO isomers are in thermal equilibrium.

Master equation calculations were carried out to evaluate the assumption that the *cis*- and *trans*-HOONO isomers are in thermal equilibrium. Calculations at 430 K and helium concentration [He] = 10^{20} cm^{-3} gave the *cis* → trans and *trans* → cis isomerization rate constants $k_{ct} = 8 \times 10^4$ s^{-1} and $k_{tc} = 6 \times 10^6$ s^{-1}, respectively. At [He] = 10^{21} cm^{-3}, the values are $k_{ct} = 2 \times 10^5$ s^{-1} and $k_{tc} = 1 \times 10^7$ s^{-1}. These rate constants can be compared to those for unimolecular decomposition of the two isomers under the same physical conditions: at [He] = 10^{20} cm^{-3}, the respective rate constants are k_{uni}(cis) = 6×10^3 s^{-1} and k_{uni}(trans) = 2×10^5 s^{-1}; at [He] = 10^{21} cm^{-3}, k_{uni}(cis) = 4×10^4 s^{-1} and k_{uni}(trans) = 2×10^6 s^{-1}. Thus, the isomerization rate is a factor of 5−10 times as fast as the decomposition rate for these conditions, supporting the assumption that cis- and *trans*-HOONO are in thermal equilibrium.

If equilibrium is measured by monitoring reactants, $K_{effective}$, the sum of both channels is obtained. $K_{effective}$ has been measured by Hippler et al.[4] for $430 < T/K < 475$. Hippler et al. interpreted their data as if there were only one form of HOONO. Using frequencies and moments of inertia estimated for this species, they report a third law value for HOONO of -10 ± 1 kJ mol^{-1}. We have interpreted their data by extracting the value of $K_{cis-cis}$ the equilibrium constant for the formation of the cis−cis isomer assuming that the ratio of isomers would be as computed from the above energies and other thermochemistry from molecular properties in Table 5 This leads to a temperature dependent "factor" by which to divide the experimental value in order to

obtain the value for just cis−cis isomer formation. From this, we compute, as shown in Table 10, a third law value of the heat of formation of the cis−cis isomer to be −8.60 kJ mol^{-1}. Using this value we compute the value of the equilibrium constant for cis−cis formation and then for trans−perp formation using the same ratios as above. (Calculations of the individual equilibrium constant for the trans−perp isomer, with heats of formation adjusted from the QCISD(T)/cc-pVDZ value relative to the value for the cis−cis isomer yield the same result, as they should.) These values are shown in Table 10. Figure 11 shows a van't Hoff plot of the Hippler et al.[4] data and the third law function deduced above. The equilibrium constants used in obtaining the recombination rate constants from the dissociation rate constants for the individual isomers are presented in Table 8.

References and Notes

(1) DeMore, W. B.; Sander, S. P.; Golden, D. M.; Hampson, R. F.; Kurylo, M. J.; Howard, C. J.; Ravishankara, A. R.; Kolb, C. E.; Molina, M. J. Chemical Kinetics and Photochemical Data for Use in Stratospheric Modeling. Evaluation Number 12; Jet Propulsion Laboratory, 1997.

(2) Atkinson, R.; Baulch, D. L.; Cox, R. A.; R. F. Hampson, J.; Kerr, J. A.; Rossi, M. J.; Troe, J. *J. Phys. Chem. Ref. Data* **1997**, *26*, 1329−499.

(3) Donahue, N. M.; Mohrschladt, R.; Dransfield, T. J.; Anderson, J. G.; Dubey, M. K. *J. Phys. Chem. A* **2001**, *105*, 1515−20.

(4) Hippler, H.; Nasterlack, S.; Striebel, F. *Phys. Chem. Chem. Phys.* **2002**, *4*, 2959−64.

(5) Robertshaw, J. S.; Smith, I. W. M. *J. Phys. Chem.* **1982**, *86*, 785−90.

(6) Burkholder, J. R.; Hammer, P. D.; Howard, C. J. *J. Phys. Chem.* **1987**, *91*, 2136−44.

(7) Golden, D. M.; Smith, G. P. *J. Phys. Chem. A* **2000**, *104*, 3991−7.

(8) Cheng, B.-M.; Lee, J.-W.; Lee, Y.-P. *J. Phys. Chem.* **1991**, *95*, 2814−7.

(9) Nizkorodov, S. A.; Wennberg, P. O. *J. Phys. Chem. A* **2002**, *106*, 855−9.

(10) Pollack, I. B.; Konen, I. M.; Li, E. X. J.; Lester, M. I. *J. Chem. Phys.* **2003**, *119*, 9981−4.

(11) Darnall, K. R.; Carter, W. P. L.; Winer, A. M.; Lloyd, A. C.; J. N. Pitts, J. *J. Phys. Chem.* **1976**, *80*, 1948−50.

(12) Atkinson, R. *J. Phys. Chem. Ref. Data* **1994**, monograph No. 2.

(13) Atkinson, R. *Atmos. Environ.* **2000**, *34*, 2063−101.

(14) Zhang, D.; Zhang, R.; Park, J.; North, S. W. *J. Am. Chem. Soc.* **2002**, *124*, 9600−5.

(15) Lohr, L. L.; Barker, J. R.; Shroll, R. M. *J. Phys. Chem. A* **2003**, *107*, 7429−33.

(16) Barker, J. R.; Lohr, L. L.; Shroll, R. M.; Reading, S. *J. Phys. Chem. A.* **2003**, *107*, 7434−44.

(17) Chakraborty, D.; Park, J.; Lin, M. C. *Chem. Phys.* **1998**, *231*, 39−49.

(18) Matheu, D. M.; Green, W. H., Jr. *Int. J. Chem. Kinet.* **2000**, *32*, 245−62.

(19) Troe, J. *Int. J. Chem. Kinet.* **2001**, *33*, 878−89.

(20) Anastasi, C.; Smith, I. W. M. *J. Chem. Soc. Faraday Trans. 2* **1976**, *72*, 1459−68.

(21) Brown, S. S.; Talukdar, R. K.; Ravishankara, A. R. *Chem. Phys. Lett.* **1999**, *299*, 277.

(22) Dransfield, T. J.; Perkins, K. K.; Donahue, N. M.; Anderson, J. G.; Sprengnether, M. M.; Demerjian, K. L. *Geophys. Res. Lett.* **1999**, *26*, 687−90.

(23) Wine, P. H.; Kreutter, N. M.; Ravishankara, A. R. *J. Phys. Chem.* **1979**, *83*, 3191−5.

(24) Fulle, D.; Hamann, H. F.; Hippler, H.; Troe, J. *J. Chem. Phys.* **1998**, *108*, 5391−7.

(25) Donahue, N. M.; Dubey, M. K.; Mohrschladt, R.; Demerjian, K. L.; Anderson, J. G. *J. Geophys. Res.* **1997**, *102*, 6159−68.

(26) D'Ottone, L.; Campuzano-Jost, P.; Bauer, D.; Hynes, A. J. *J. Phys. Chem. A* **2001**, *105*, 10538−43.

(27) McGrath, M. P.; Francl, M. M.; Rowland, F. S.; Hehre, W. J. *J. Phys. Chem.* **1988**, *88*, 5352.

(28) McGrath, M. P.; Rowland, F. S. *J. Phys. Chem.* **1994**, *98*, 1061−7.

(29) Morris, V.; Bhatia, S. C.; Hall, J. H., Jr. *J. Phys. Chem.* **1990**, *90*, 7414.

(30) Palmer, M. H. *J. Mol. Struct.* **1990**, *239*, 173.

(31) Koppenol, W.; Klasinc, L. *Int. J. Quantum Chem.* **1993**, *20*, 1.

(32) Tsai, H.-H. M.; Harrison, J. G.; Martin, J. C.; Hamilton, T. P.; Woerd, M. v. d.; Jablonsky, M. J.; Beckman, J. S. *J. Am. Chem. Soc.* **1994**, *116*, 4115.

(33) Tsai, H.-H.; Hamilton, T. P.; Tsai, J.-H. M.; van der Woerd, M.; Harrison, J. G.; Jablonsky, M. J.; Beckman, J. S.; Koppenol, W. E. *J. Phys. Chem.* **1996**, *100*, 15087.

(34) Krauss, M. *Chem. Phys. Lett.* **1994**, *222*, 513.

(35) Cameron, D. R.; Borrajo, A. M. P.; Bennett, B. M.; Thatcher, G. R. J. *Can. J. Chem.* **1995**, *73*, 1627.

(36) Jursic, B. S. *J. Mol. Struct.* **1996**, *370*, 65.

(37) Houk, K. N.; Condroski, K. R.; Pryor, W. A. *J. Am. Chem. Soc.* **1996**, *118*, 13002.

(38) Sumathy, R.; Peyerimhoff, S. D. *J. Chem. Phys.* **1997**, *107*, 1872−80.

(39) Li, Y.; Francisco, J. S. *J. Chem. Phys.* **2000**, *113*, 7976−81.

(40) Dixon, D. A.; Feller, D.; Zhan, C.-G.; Francisco, J. S. *J. Phys. Chem. A* **2002**, *106*, 3191−6.

(41) Frisch, M. J.; Trucks, G. W.; Schlegel, H. B.; Gill, P. M. W.; Johnson, B. G.; Robb, M. A.; Cheeseman, J. R.; Keith, T.; Petersson, G. A.; Montgomery, J. A.; Raghavachari, K.; Al-Laham, M. A.; Zakrzewski, V. G.; Ortiz, J. V.; Foresman, J. B.; Cioslowski, J.; Stefanov, B. B.; Nanayakkara, A.; Challacombe, M.; Peng, C. Y.; Ayala, P. Y.; Chen, W.; Wong, M. W.; Andres, J. L.; Replogle, E. S.; Gomperts, R.; Martin, R. L.; Fox, D. J.; Binkley, J. S.; Defrees, D. J.; Baker, J.; Stewart, J. P.; Head-Gordon, M.; Gonzalez, C.; Pople, J. A. *Gaussian 94*, revision B.3; Gaussian, Inc.: Pittsburgh, PA, 1995.

(42) Frisch, M. J.; Trucks, G. W.; Schlegel, H. B.; Scuseria, G. E.; Robb, M. A.; Cheeseman, J. R.; Zakrzewski, V. G.; Montgomery, J. A., Jr.; Stratmann, R. E.; Burant, J. C.; Dapprich, S.; Millam, J. M.; Daniels, A. D.; Kudin, K. N.; Strain, M. C.; Farkas, O.; Tomasi, J.; Barone, V.; Cossi, M.; Cammi, R.; Mennucci, B.; Pomelli, C.; Adamo, C.; Clifford, S.; Ochterski, J.; Petersson, G. A.; Ayala, P. Y.; Cui, Q.; Morokuma, K.; Malick, D. K.; Rabuck, A. D.; Raghavachari, K.; Foresman, J. B.; Cioslowski, J.; Ortiz, J. V.; Stefanov, B. B.; Liu, G.; Liashenko, A.; Piskorz, P.; Komaromi, I.; Gomperts, R.; Martin, R. L.; Fox, D. J.; Keith, T.; Al-Laham, M. A.; Peng, C. Y.; Nanayakkara, A.; Gonzalez, C.; Challacombe, M.; Gill, P. M. W.; Johnson, B. G.; Chen, W.; Wong, M. W.; Andres, J. L.; Head-Gordon, M.; Replogle, E. S.; Pople, J. A. *Gaussian 98*, revision A.1x; Gaussian, Inc.: Pittsburgh, PA, 1998.

(43) Ellison, G. B.; Blanksby, S. J.; Jochnowitz, E. B.; Stanton, J. F. *J. Phys. Chem. A*, in preparation.

(44) Wagman, D. D.; Evans, W. H.; Parker, V. B.; Schumm, R. H.; Halow, I.; Bailey, S. M.; Churney, K. L.; Nuttall, R. L. *J. Phys. Chem. Ref. Data* **1982**, *11*, 1.

(45) Ruscic, B.; Feller, D.; Dixon, D. A.; Peterson, K. A.; Harding, L. B.; Asher, R. L.; Wagner, A. F. *J. Phys. Chem. A* **2001**, *105*, 1−4.

(46) Ruscic, B.; Wagner, A. F.; Harding, L. B.; Asher, R. L.; Feller, D.; Dixon, D. A.; Peterson, K. A.; Song, Y.; Qian, X.; Ng, C.-Y.; Liu, J.; Chen, W.; Schwenke, D. W. *J. Phys. Chem. A* **2002**, *106*, 2727−47.

(47) Bauschlicher, C. W., Jr.; Partridge, H. *Chem. Phys. Lett.* **1993**, *208*, 241.

(48) Lide, D. R. *CRC Handbook of Chemistry and Physics*, 81st ed.; CRC Press: Boca Raton, 2000.

(49) Forst, W. *Theory of Unimolecular Reactions*; Academic Press: New York, 1973.

(50) Gilbert, R. G.; Smith, S. C. *Theory of Unimolecular and Recombination Reactions*; Blackwell Scientific: Oxford, 1990.

(51) Barker, J. R. *Int. J. Chem. Kinet.* **2001**, *33*, 232−45.

(52) Barker, J. R.; Ortiz, N. F. *Int. J. Chem. Kinet.* **2001**, *33*, 246−61.

(53) Barker, J. R. MultiWell Program Suite (1.3.2); 1.3.2 ed.; http://aoss.engin.umich.edu/multiwell/: Ann Arbor, MI, 2003.

(54) Robinson, P. J.; Holbrook, K. A. *Unimolecular Reactions*; Wiley-Interscience: New York, 1972.

(55) Beyer, T.; Swinehart, D. F. *Comm. Assoc. Comput. Machines* **1973**, *16*, 379.

(56) Stein, S. E.; Rabinovitch, B. S. *J. Chem. Phys.* **1973**, *58*, 2438−45.

(57) Holbrook, K. A.; Pilling, M. J.; Robertson, S. H. *Unimolecular Reactions*, 2nd ed.; Wiley: Chichester, 1996.

(58) Truhlar, D. G.; Garrett, B. C. *Acc. Chem. Res.* **1980**, *13*, 440−8.

(59) Benson, S. W. *Thermochemical Kinetics*, 2nd ed.; Wiley: New York, 1976.

(60) Smith, G. P.; Golden, D. M. *Int. J. Chem. Kinet.* **1978**, *10*, 489.

(61) Gorin, E. *Acta Physicochim., URSS* **1938**, *9*, 691.

(62) Atkinson, R.; Aschmann, S. M.; Carter, P. L.; Pitts, J. N., Jr. *J. Phys. Chem.* **1982**, *86*, 4563−69.

(63) Ranschaert, D. L.; Schneider, N. J.; Elrod, M. J. *J. Phys. Chem. A* **2000**, *104*, 5758−65.

(64) Scholtens, K. W.; Messer, B. M.; Kappa, C. D.; Elrod, M. J. *J. Phys. Chem. A* **1999**, *103*, 4378−84.

(65) NIST. *Chemistry WebBook: NIST Standard Reference Database Number 69*; March 2003 ed.; National Institute of Science and Technology, 2003.

(66) Barker, J. R.; Yoder, L. M.; King, K. D. *J. Phys. Chem. A* **2001**, *105*, 796−809.
(67) Maergoiz, A. I.; Nikitin, E. E.; Troe, J.; Ushakov, V. G. *J. Chem. Phys.* **1998**, *108*, 9987−98.
(68) Maergoiz, A. I.; Nikitin, E. E.; Troe, J.; Ushakov, V. G. *J. Chem. Phys.* **1998**, *108*, 5265−80.
(69) Troe, J. *J. Chem. Phys.* **1977**, *66*, 4758−75.
(70) Troe, J. *J. Chem. Phys.* **1977**, *66*, 4745−57.
(71) Steinfeld, J. I.; Francisco, J. S.; Hase, W. L. *Chemical Kinetics and Dynamics*, 2nd ed.; Prentice-Hall: 1998.
(72) Oref, I. *J. Phys. Chem.* **1989**, *93*, 3465−9.
(73) Hessler, J. P.; Ogren, P. J. *J. Phys. Chem.* **1996**, *100*, 984−92.
(74) Pilling, M. J. *Int. J. Chem. Kinet.* **1989**, *21*, 267−91.
(75) Pawlowska, I. Z.; Gardiner, W. C.; Oref, I. *J. Phys. Chem.* **1993**, *97*, 5024−31.
(76) Kazakov, A.; Wang, H.; Frenklach, M. *J. Phys. Chem.* **1994**, *98*, 10598−605.
(77) Wang, H.; Frenklach, M. *Chem. Phys. Lett.* **1993**, *205*, 271−76.
(78) Hessler, J. P. *J. Phys. Chem.* **1996**, *100*, 2141−44.
(79) Prezhdo, O. *J. Phys. Chem.* **1995**, *99*, 8633−7.
(80) Marquardt, D. W. *J. Soc. Ind. Appl. Math.* **1963**, *11*, 431.
(81) Press: W. H.; Teukolsky, S. A.; Vetterling, W. T.; Flannery, B. P. Levenberg−Marquardt Methodol. In *Numerical Recipes in FORTRAN The Art of Scientific Computing* 2nd ed.; Cambridge University Press: New York, 1992; Vol. 1, pp 678−83.
(82) Synergy. KaleidaGraph; 3.51 ed.; Synergy Software, 2001.
(83) Yu, X.-Y.; Barker, J. R. *J. Phys. Chem. A* **2003**, *107*, 1313−24.
(84) Yu, X.-Y.; Barker, J. R. *J. Phys. Chem. A* **2003**, *107*, 1325−32.
(85) Sander, R.; Crutzen, P. J. *J. Geophys. Res.* **1996**, *101*, 9121−38.
(86) Seinfeld, J. H.; Pandis, S. N. *Atmospheric Chemistry and Physics*; John Wiley & Sons: New York, 1998.
(87) Finlayson-Pitts, B. J.; Pitts, J. N., Jr. *Chemistry of the Upper and Lower Atmosphere*; Academic Press: San Diego, 2000.
(88) 1976 Standard Atmosphere Calculator; Digital Dutch, 2003.
(89) *U. S. Standard Atmosphere, 1976*; U.S. Government Printing Office: Washington, DC, 1976.